PIER Letters

(Received 20 November 2024, Accepted 7 January 2025, Scheduled 23 January 2025)

High Gain Dual-Frequency Dual-Circularly Polarized Fabry Perot Resonant Cavity Antenna for Ku Band

Wei Luo[1,*], Xiaoxue Wang[1], Xin He[1], and Yuqi Yang[2]

[1] *School of Optoelectronic Engineering, Chongqing University of Posts and Telecommunications, Chongqing, China*
[2] *Electromagnetic Field and Wireless Technology Innovation Team*
Chongqing University of Posts and Telecommunications, Chongqing, China

ABSTRACT: To explore higher-performance satellite communication antennas, a dual-frequency dual-circularly polarized antenna based on a Fabry-Perot (F-P) resonant cavity is proposed in this letter. An artificial magnetic conductor (AMC) is loaded onto the resonant cavity as a partial reflection surface (PRS) to reduce the profile. The electromagnetic (EM) waves from the feeder are reflected multiple times within the cavity and subsequently superimposed in phase, thereby enabling dual-frequency operation and high gain. Right-handed circularly polarized (RHCP) and left-handed circularly polarized (LHCP) waves are respectively generated in the lower and higher frequency bands by incorporating a dual-frequency polarization conversion surface (PCS). Two rectangular microstrip patch antennas with a simple feeding network are employed as the feeder for RHCP and LHCP, respectively. The measurement results show that the operating bandwidth is 4.77% (12.47–13.08 GHz) for the low-frequency band and 5.36% (16.51–17.42 GHz) for the high-frequency band. The maximum gains of 14.91 dBi and 14.33 dBi are achieved for the lower and higher frequency bands, respectively. The proposed antenna fulfills the requirements of the frequency division duplex satellite communication system, providing a promising candidate for ground equipment in high-speed satellite Internet applications.

1. INTRODUCTION

Mobile communication standards have evolved into the new era of beyond fifth-generation (B5G) and sixth-generation (6G). The integration of satellite communication with ground mobile communication networks has become an important development trend [1]. Furthermore, satellite communication has demonstrated significant performance in numerous scenarios, encompassing wide-area Internet of Things (IOT), high-precision positioning and navigation, real-time Earth observation, and broadband services in areas without network coverage [2, 3]. Antennas characterized by dual-circular polarization and high-gain radiation capabilities are indispensable for satellite communication. The antenna enhances performance in multipath environments. It effectively mitigates interference in complex electromagnetic environments [4, 5], efficiently receives circularly polarized signals from satellites, and reduces interference from ground-reflected signals in satellite communication systems, thereby improving communication quality. Meanwhile, compared to dielectric lens antenna and parabolic antennas [6, 7], Fabry-Perot (F-P) resonant cavity antenna is recognized as a typical high-gain antenna. It is characterized by a low profile, simple structure, and low cost, making it easier to integrate and produce [8]. Furthermore, compared with phased array antennas [9], which often incorporate complex feeding networks, F-P resonant cavity antennas usually adopt a single-feed form, without considering the serious coupling and radiation losses caused by the feeding network. Consequently, it holds great potential for application in the field of satellite communication.

In addition, leveraging the capability of metasurfaces to manipulate electromagnetic waves, numerous studies have been conducted to enhance antenna performance by incorporating metasurface structures into antenna designs [10–14]. The pivotal technology of the F-P resonant cavity antenna resides in the employment of electromagnetic (EM) metasurface technology for constructing the resonant cavity. This approach facilitates the achievement of high gain, low profile, circular polarization, and other advantageous performances [15–18]. A dual-circular polarization F-P resonant cavity antenna, equipped with a self-polarizing partial reflection surface (PRS) was proposed, achieving a maximum gain of 13.7 dBi and an operating bandwidth of 8.6% [17]. A dual-circular polarization F-P resonant cavity antenna loaded with a polarizer was designed, featuring a maximum gain and operating bandwidth of 17.2 dBi and 4.0%, respectively [19]. Recently, research has highlighted a trade-off between gain and bandwidth in dual-frequency, dual-circularly polarized F-P resonant cavity antennas, necessitating further research and development in this area.

In this letter, a dual-frequency, dual-circularly polarized F-P resonant cavity antenna is proposed, which utilizes a double-layer printed artificial magnetic conductor (AMC) as the partially reflecting layer within the cavity. Dual-frequency resonance is achieved within a single cavity by the high-order mode of the F-P resonant cavity, and the profile height of the antenna is reduced. A dielectric disk is loaded inside the cavity to op-

* Corresponding author: Wei Luo (luowei1@cqupt.edu.cn).

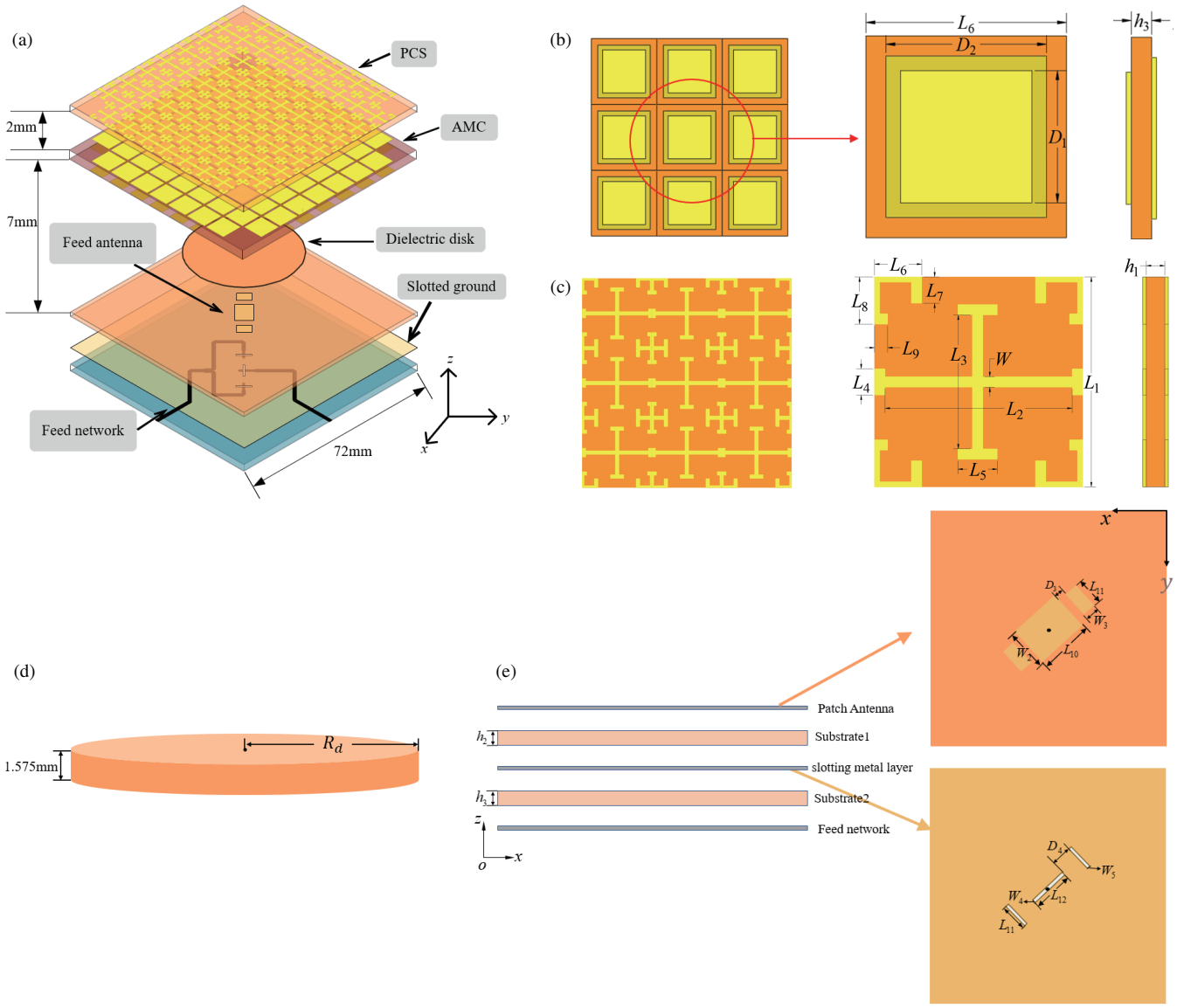

FIGURE 1. Schematic diagram of the proposed antenna. (a) Overall structure diagram of antenna. (b) AMC structure. (c) PCS structure. (d) The dielectric disk structure. (e) The feed antenna structure.

timize the electric field distribution inside the cavity, thereby expanding the gain bandwidth of the antenna. Dual-circular polarization is realized by incorporating a polarization conversion surface (PCS), rather than depending on the polarization type of the feed source, thus improving the complexity of the feed network of the feed source. The proposed antenna exhibits good bandwidth and circularly polarized radiation performance, making it suitable for the use in satellite communication ground terminals.

2. ANTENNA GEOMETRY AND ANALYSIS

2.1. Antenna Configuration

The structure of the proposed antenna is shown in Figure 1, which comprises a PCS, an AMC, a dielectric disk, a feeder, and a slotted ground. The key structural parameters of the antenna are presented in Table 1. The AMC serves as the partially reflecting layer, consisting of two metallic layers separated by Rogers 4003 ($\varepsilon_r = 3.55$) with a thickness of 0.813 mm. The slotted ground and AMC form a dual-frequency F-P resonant cavity. This configuration maintains a low profile while enhancing the gain of the dual-band system. The crossed "I"-shaped structures are etched onto two sides of F4B ($\varepsilon_r = 2.20$) with a height of 3.00 mm to form PCS, which is used to convert the polarization of the EM waves from the feeder. Both of AMC and PCS consist of 9×9 units, all of which have the same period and correspond to each other on a one-to-one basis. A dielectric disk of Rogers 5880 ($\varepsilon_r = 2.20$) is inserted into the cavity to optimize the electric field distribution within it, thereby broadening the operational bandwidth of the lower frequency band. The feeder consists of a low-frequency patch antenna and a high-frequency patch antenna array, which are excited by the feed network located at the bottom layer of the feeder through the coupling slots in the ground. The slotting metal layer in the

TABLE 1. Structural parameters of proposed antenna (unit: mm).

Para	h	h_1	h_2	h_3	D_1	D_2	D_3	D_4	L
Value	0.813	3	1.575	0.4	8	8	7.2	5.1	8
Para	L_1	L_2	L_3	L_4	L_5	L_6	L_7	L_8	L_9
Value	8	7.2	5.1	1	1.5	2.8	2	2.8	1
Para	L_{10}	L_{11}	L_{12}	W	W_2	W_3	W_4	W_5	
Value	8	4.6	5.8	0.4	6	3.9	0.4	0.3	

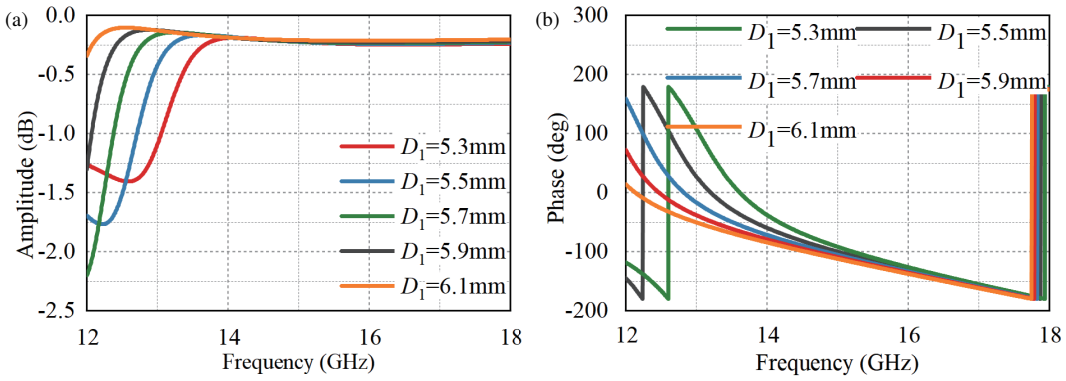

FIGURE 2. The relationship between D_1 and the reflection coefficient of AMC. (a) Reflection amplitude. (b) Reflection phase.

middle is separated by substrate1 of Rogers 5880 and substrate2 of FR-4 ($\varepsilon_r = 4.4$), as shown in Figure 1(e). The feeder is rotated by 45° to ensure that the x-polarization and y-polarization components from the feeder are equal. A unit is removed from each corner of the AMC and PCS to facilitate fixation and installation. The antenna is installed and fixed with plastic screws and nuts through the holes drilled at each corner of the AMC and PCS.

2.2. Analysis of the AMC

The relationship between the resonant frequency of the F-P resonant cavity antenna f_0 and the height of cavity h can be expressed by:

$$h = \frac{(\varphi_s + \varphi_g + 2N\pi)C}{4\pi f_0} \quad N = 0, 1, 2 \ldots \tag{1}$$

where φ_g is the reflection phase of the ground, and N is the resonant mode. Assuming that φ_g equals 180°, the reflection phase of AMC φ_s determines the resonant frequency of the F-P cavity when the height of the resonant cavity h is fixed. Multi-frequency function can be achieved by the F-P resonant cavity when the solution between φ_s and f_0 is not unique. The relationship between φ_s and f_0 in the low- and high-frequencies can be expressed by:

$$\begin{cases} h_L = \dfrac{C}{4\pi f_L}(\varphi_L + \pi) \\ h_H = \dfrac{C}{4\pi f_H}(\varphi_H + \pi) \end{cases} \tag{2}$$

where f_L and f_H represent the low and high frequencies, respectively. φ_L and φ_H represent the reflection phases of the AMC at low-frequency and high-frequency, respectively. The F-P resonant cavity achieves dual-frequency resonance when $h_L = h_H$. The relationship between φ_L and φ_H is expressed by:

$$\varphi_L = \frac{f_L}{f_H}(\varphi_H + \pi) - \pi \tag{3}$$

The dual-frequency resonance can be achieved by a single F-P cavity when the adjustable range of φ_H satisfies the Equation (3) as long as φ_H is fixed. The relationship between D_1 and the reflection coefficient of AMC is shown in Figure 2. The phase in the higher frequency band remains unchanged with the increase of D_1 while the phase in low-frequency decreases within a certain range, which indicates the dual-frequency resonance in the F-P resonant cavity.

2.3. Analysis of the PCS

Due to the different sensitivities of the orthogonal "I"-shaped structure to EM waves with different polarizations, it is possible to independently manipulate vertical and horizontal EM waves [17]. To provide a more intuitive view of the polarization conversion characteristics of PCS, Figure 3 shows the surface current maps of the PCS at 13.21 GHz and 17.38 GHz during one cycle. At 13.21 GHz, the current is mainly concentrated in the central "I" shape, and at 17.38 GHz, the current is mainly concentrated in the "I" shape around it. It can be seen that when the cycle goes from 0 to T, the surface current of the PCS rotates counterclockwise at low frequencies and

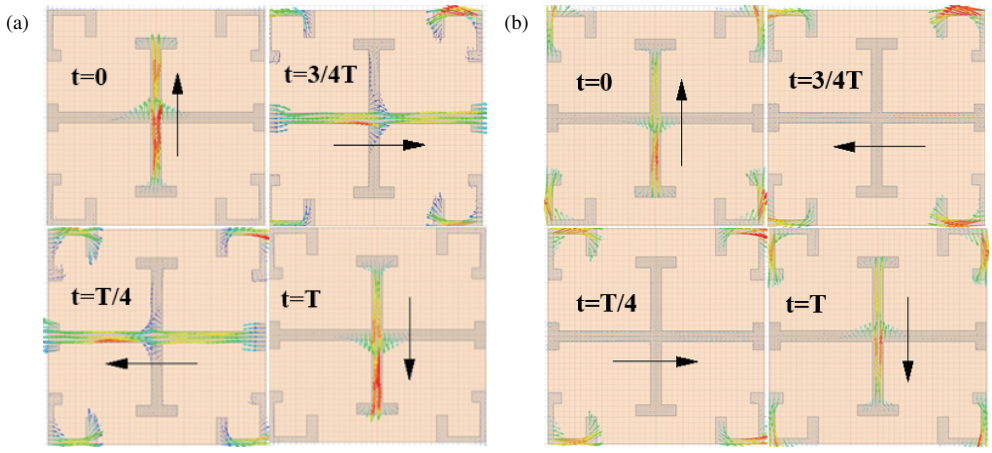

FIGURE 3. PCS surface current distribution at low frequency and high frequency. (a) 13.21 GHz. (b) 17.38 GHz.

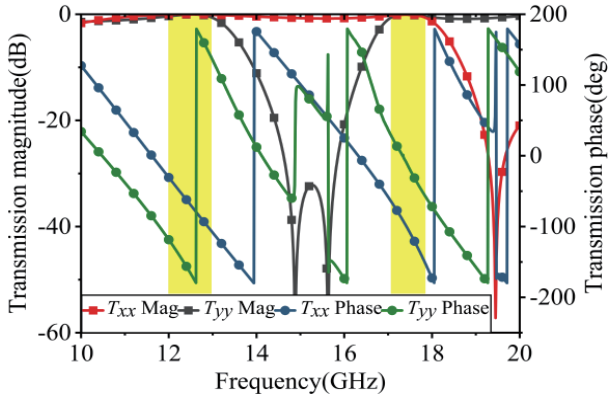

FIGURE 4. The transmission coefficient curve of the proposed PCS and polarization conversion frequency band.

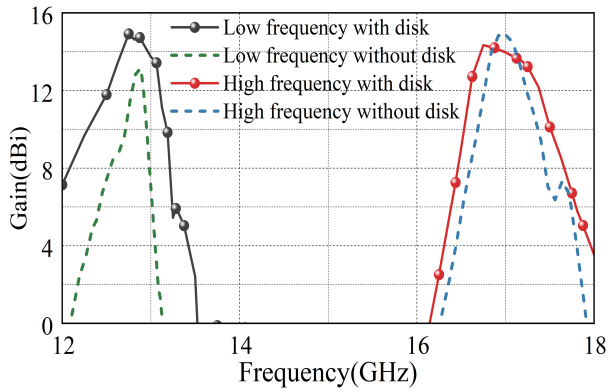

FIGURE 5. The influence of dielectric disk on the gain of F-P resonant cavity antenna.

clockwise at high frequencies. The PCS element is shown in Figure 1(c). The crossed "I"-shaped structures are etched onto both sides of the substrate with the same structural parameters. When the amplitude of the co-polarization transmission coefficients T_{xx} and T_{yy} are equal, and the phase difference of T_{xx} and T_{yy} is ±90°, two orthogonal linear waves are converted to circularly polarized waves. The co-polarization transmission coefficients of the PCS are shown in Figure 4. In both the low-frequency range (12.44 GHz to 13.36 GHz) and high-frequency range (16.71 GHz to 17.46 GHz), the magnitude difference of the transmission coefficient S_{21} for x- and y-polarized incident waves is less than 0.5 dB, and the phase difference lies within 90° ±15°. The amplitudes of T_{xx} and T_{yy} are approximately equal while the phase difference of T_{xx} and T_{yy} is 90° in the highlighted area. The polarization of transmitted EM wave is simultaneously converted by the PCS in the two frequency bands.

2.4. Dielectric Disk Insertion

As depicted in Figure 2(b), the reflection phase of the artificial magnetic conductor (AMC) undergoes a rapid change in the lower frequency band. This rapid change subsequently results in a narrowing of the antenna's bandwidth, according to Equation (3). Therefore, loading the dielectric disk into the cavity aims to expand the low-frequency bandwidth of the antenna by optimizing the electric field distribution at low frequencies. The effects of the dielectric disk on the gain and bandwidth of the antenna are shown in Figure 5. After loading the dielectric disk, the 3 dB gain bandwidth of the antenna at the low-frequency range is 12.51 GHz to 13.10 GHz (4.61%), and at the high-frequency range it is 16.58 GHz to 17.43 GHz (5.00%). The peak gain at 12.80 GHz is 14.93 dBi, and the peak gain at 16.80 GHz is 14.33 dBi. The bandwidth of the lower frequency band is expanded with the addition of the dielectric disk. Additionally, the effects of the dielectric disk on the electric field distribution of the antenna are depicted in Figure 6. After inserting the dielectric disk, the electric field distribution within the cavity becomes more uniform, which suggests that the operating bandwidth of the antenna in the lower frequency band has been improved.

3. MEASUREMENTS AND DISCUSSION

The prototype has been fabricated and measured to verify the performance of the designed antenna. The PCS, PRS, and feeder of the antenna are fixed with plastic screws, and the antenna is fed through an SMA interface. The prototype is

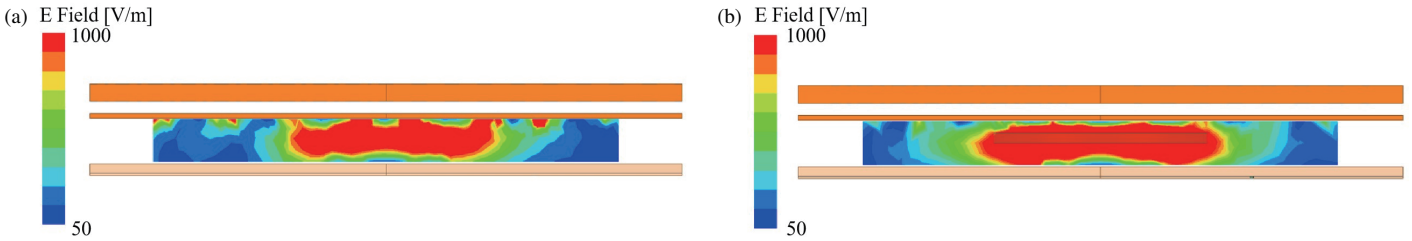

FIGURE 6. Distribution of electric field in the cavity of F-P resonant cavity antenna operating at low frequencies. (a) Without disk insertion, and (b) with disk insertion.

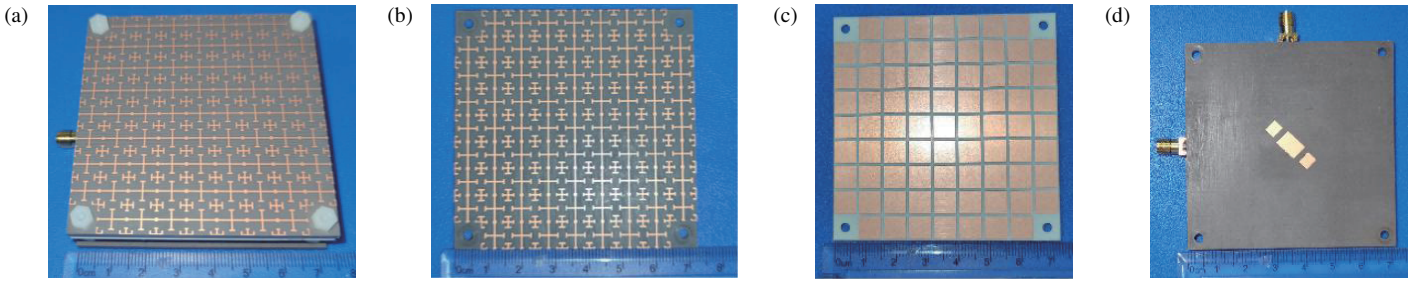

FIGURE 7. Proposed antenna prototype. (a) Side view, (b) PCS layer, (c) PRS layer, and (d) feeder.

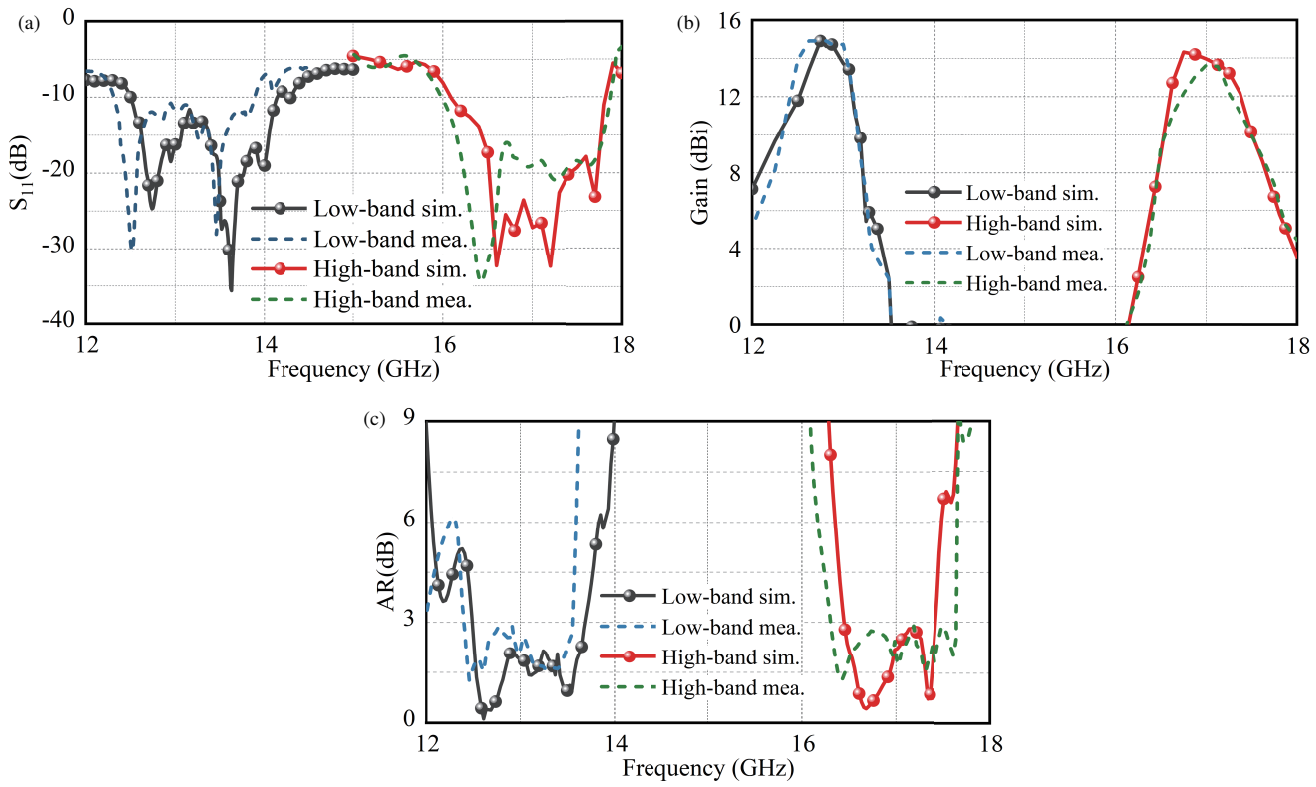

FIGURE 8. Comparison between measurements and simulations. (a) S_{11}, (b) gain, and (c) axial ratio (AR).

shown in Figure 7. The measurement and simulation results are compared in Figure 8. The slight deviation of the measured impedance towards low frequencies and the lower axial ratio, as compared to simulations, are attributed to welding and assembly errors, coupled with inadequate machining accuracy. The measured gain exhibits a slight decrease, influenced by the thickness of the cavity and deformation of the dielectric plate in practical measurements. The measured relative impedance bandwidths are 11.98% (12.32–13.89 GHz) and 10.99% (16.00–17.86 GHz) for the lower and higher frequency bands, respectively. The 3 dB gain bandwidths measured are 5.66% (12.36–13.08 GHz) for the low-frequency band

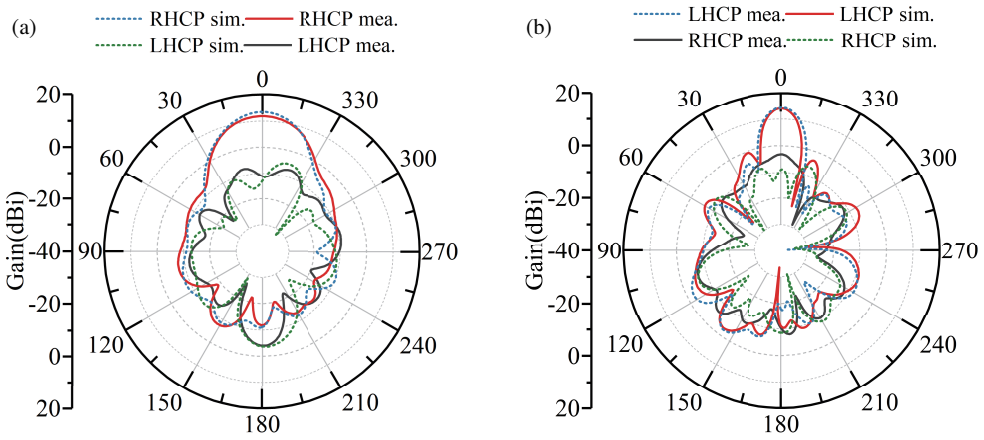

FIGURE 9. Measurement and simulation patterns of F-P resonant cavity antenna. (a) 12.80 GHz and (b) 17.00 GHz.

TABLE 2. Comparison between this paper and references.

Ref.	Polarization	Freq. (GHz)	BW (%)	AR BW (%)	Peak Gain (dBi)	Radiator Height (λ_0)
[17]	Single-band Dual-CP	5.80	13.8/13.1	8.60	13.70	0.58
[20]	Single-band Dual-CP	27.95	5.40/5.76	5.30/4.30	16.85/17.20	0.76
[21]	Dual-band dual-CP	2.36/4.15	2.70/2.40	2.70/2.40	7.10/10.00	0.47
[22]	Dual-band dual-CP	7.30	1.10/2.50	1.10/2.50	12.98/13.25	0.55
[23]	Single-band Dual-CP	10.00	2.80	5.00	13.40/13.40	0.36
This work	Dual-band dual-CP	12.80/17.00	4.77/5.36	9.05/7.95	14.91/14.08	0.42

and 5.48% (16.51–17.44 GHz) for the high-frequency band, as shown in Figure 8(b). The 3 dB axial ratio bandwidths of 9.02% (12.39–13.56 GHz) and 7.95% (16.30–17.65 GHz) are achieved in the low- and high-frequencies, respectively. Taking the intersection of the aforementioned bandwidths as the operating bandwidth, the operating bandwidths of the antenna are 4.77% (12.47–13.08 GHz) and 5.36% (16.51–17.42 GHz). The maximum gains of the antenna are 14.91 dBi and 14.08 dBi in the low- and high-frequency bands, respectively. The measured and simulated radiation patterns are shown in Figure 9, which indicates that the measurement and simulation are in good agreement.

Table 2 presents the comparison between the proposed antenna and previous circularly polarized F-P resonant cavity antennas. It can be seen that compared with other dual frequency dual circularly polarized antennas [20, 21], the F-P resonant cavity antenna designed in this paper has better measured gain bandwidth. Compared to [18], the gain bandwidth still needs further improvement, but peak gain and radiation height have certain advantages. Overall, this article focuses more on improving gain bandwidth while ensuring performance such as peak gain and radiation height. Notably, the proposed antenna exhibits dual-frequency and dual-circularly polarized radiation performance, along with certain advantages in terms of operating bandwidth and gain.

4. CONCLUSION

A novel F-P resonant cavity antenna with metasurface is proposed, whose operating bandwidth is improved by inserting a dielectric disk. The dual-frequency resonance is designed by just one cavity with the help of an AMC, and RHCP and LHCP transmitted waves are generated with PCS for different bands. The crucial limitation of the proposed Fabry-Perot resonant cavity antenna is the contradiction between gain and impedance matching. Considering the trade-off between antenna gain and bandwidth, the gain bandwidth of the proposed antenna can be further expanded by optimizing the PCS element and height of resonance cavity. Notably, the merits of the high-gain and dual-frequency dual-circular polarization radiation performance make the antenna a promising candidate for fixed satellite service and broadcasting satellite service mobile end of satellite communication.

ACKNOWLEDGEMENT

This work was supported in part by the China Postdoctoral Science Foundation under Grant 2022MD723726 and Opening Project of Guangxi Wireless Broadband Communication and Signal Processing Key Laboratory under Grant GXKL06230206.

REFERENCES

[1] Chen, S., S. Sun, and S. Kang, "System integration of terrestrial mobile communication and satellite communication — The trends, challenges and key technologies in B5G and 6G," *China Communications*, Vol. 17, No. 12, 156–171, 2020.

[2] Li, J., Y. Hu, L. Xiang, W. Kong, and W. Hong, "Broadband circularly polarized magnetoelectric dipole antenna and array for K-band and Ka-band satellite communications," *IEEE Transactions on Antennas and Propagation*, Vol. 70, No. 7, 5907–5912, 2022.

[3] Ran, J., Y. Wu, C. Jin, P. Zhang, and W. Wang, "Dual-band multipolarized aperture-shared antenna array for Ku-/Ka-band satellite communication," *IEEE Transactions on Antennas and Propagation*, Vol. 71, No. 5, 3882–3893, 2023.

[4] Wang, H. B. and Y. J. Cheng, "Single-layer dual-band linear-to-circular polarization converter with wide axial ratio bandwidth and different polarization modes," *IEEE Transactions on Antennas and Propagation*, Vol. 67, No. 6, 4296–4301, 2019.

[5] Wang, H. B., Y. J. Cheng, and Z. N. Chen, "Dual-band miniaturized linear-to-circular metasurface polarization converter with wideband and wide-angle axial ratio," *IEEE Transactions on Antennas and Propagation*, Vol. 69, No. 12, 9021–9025, 2021.

[6] Fang, S., L. Zhang, Y. Guan, Z. Weng, and X. Wen, "A wideband Fabry-Pérot cavity antenna with single-layer partially reflective surface," *IEEE Antennas and Wireless Propagation Letters*, Vol. 22, No. 2, 412–416, 2023.

[7] Liu, X., Z. Yan, E. Wang, T. Zhang, and F. Fan, "Magnetoelectric dipole-fed Fabry-Pérot antenna with wideband RCS reduction based on multilayer metasurface," *IEEE Antennas and Wireless Propagation Letters*, Vol. 20, No. 7, 1342–1346, 2021.

[8] Liu, Z., J. Bornemann, S. Liu, and X. Kong, "Investigations and prospects of Fabry-Pérot antennas: A review," *Journal of Systems Engineering and Electronics*, Vol. 32, No. 4, 731–747, 2021.

[9] Lee, G. H., S. Kumar, H. C. Choi, and K. W. Kim, "Wideband high-gain double-sided dielectric lens integrated with a dual-bowtie antenna," *IEEE Antennas and Wireless Propagation Letters*, Vol. 20, No. 3, 293–297, 2020.

[10] Taravati, S. and G. V. Eleftheriades, "Microwave space-time-modulated metasurfaces," *ACS Photonics*, Vol. 9, No. 2, 305–318, 2022.

[11] Xu, P., H. W. Tian, W. X. Jiang, Z. Z. Chen, T. Cao, C.-W. Qiu, and T. J. Cui, "Phase and polarization modulations using radiation-type metasurfaces," *Advanced Optical Materials*, Vol. 9, No. 16, 2100159, 2021.

[12] Cao, T., K. Liu, Y. Tang, J. Deng, K. Li, and G. Li, "A high-index $Ge_2Sb_2Te_5$-based Fabry-Pérot cavity and its application for third-harmonic generation," *Laser & Photonics Reviews*, Vol. 13, No. 7, 1900063, 2019.

[13] Bao, J., N. Liu, H. Tian, *et al.*, "Chirality enhancement using Fabry-Pérot-like cavity," *Research*, Vol. 2020, 7873581, 2020.

[14] Forouzmand, A. and H. Mosallaei, "A tunable semiconductor-based transmissive metasurface: Dynamic phase control with high transmission level," *Laser & Photonics Reviews*, Vol. 14, No. 6, 1900353, 2020.

[15] Zhu, J., Y. Yang, S. Liao, S. Li, and Q. Xue, "Dual-band aperture-shared Fabry-Pérot cavity-integrated patch antenna for millimeter-wave/sub-6 GHz communication applications," *IEEE Antennas and Wireless Propagation Letters*, Vol. 21, No. 5, 868–872, 2022.

[16] Guan, Y., Y.-C. Jiao, Y.-D. Yan, Y. Feng, Z. Weng, and J. Tian, "Wideband and compact Fabry-Pérot resonator antenna using partially reflective surfaces with regular hexagonal unit," *IEEE Antennas and Wireless Propagation Letters*, Vol. 20, No. 6, 1048–1052, 2021.

[17] Niaz, M. W., Y. Yin, R. A. Bhatti, Y.-M. Cai, and J. Chen, "Wideband Fabry-Pérot resonator antenna employing multilayer partially reflective surface," *IEEE Transactions on Antennas and Propagation*, Vol. 69, No. 4, 2404–2409, 2021.

[18] Jeon, Y.-G., G.-R. Yun, J. Kim, and D. Kim, "Polarization reconfigurable high-gain Fabry-Pérot cavity antenna," *IEEE Transactions on Antennas and Propagation*, Vol. 70, No. 9, 7727–7734, 2022.

[19] Le, H. D., T. Le-Huu, K. K. Nguyen, and S. X. Ta, "Dual circularly-polarized Fabry-Pérot antenna using single-layer self-polarizing PRS," *IEEE Antennas and Wireless Propagation Letters*, Vol. 22, No. 10, 2575–2579, 2023.

[20] Li, Y.-L. and K.-M. Luk, "Dual circular polarizations generated by self-polarizing Fabry-Pérot cavity antenna with loaded polarizer," *IEEE Transactions on Antennas and Propagation*, Vol. 69, No. 12, 8890–8898, 2021.

[21] Wang, P., J. Liu, C. Zhou, B. Yin, and W. Wang, "Dual-band dual-circularly polarized Fabry-Pérot cavity MIMO antenna using CMM-based polarization converter and MMA for vehicular satellite communications," *IEEE Transactions on Vehicular Technology*, Vol. 72, No. 7, 8844–8856, 2023.

[22] Chen, C., Z.-G. Liu, H. Wang, and Y. Guo, "Metamaterial-inspired self-polarizing dual-band dual-orthogonal circularly polarized Fabry-Pérot resonator antennas," *IEEE Transactions on Antennas and Propagation*, Vol. 67, No. 2, 1329–1334, 2019.

[23] Wang, Y. and A. Zhang, "Dual circularly polarized fabry-pérot resonator antenna employing a polarization conversion metasurface," *IEEE Access*, Vol. 9, 44 881–44 887, 2021.